Hindawi
Mathematical Problems in Engineering
Volume 2020, Article ID 5251804, 15 pages
https://doi.org/10.1155/2020/5251804

Research Article

Impact of Activation Energy and Temperature-Dependent Heat Source/Sink on Maxwell–Sutterby Fluid

T. Sajid,[1] **S. Tanveer**,[2] **Z. Sabir**,[3] **and J. L. G. Guirao**[4]

[1]*Department of Mathematics, Capital University of Science and Technology, Islamabad, Pakistan*
[2]*Department of Mathematics, Government Degree College for Women, Fatehjang, Attock, Pakistan*
[3]*Department of Mathematics and Statistics, Hazara University, Mansehra, Pakistan*
[4]*Department of Applied Mathematics and Statistics, Technical University of Cartagena, Hospital de Marina, 30203 Cartagena, Spain*

Correspondence should be addressed to J. L. G. Guirao; juan.garcia@upct.es

Received 15 March 2020; Revised 25 May 2020; Accepted 13 July 2020; Published 4 August 2020

Academic Editor: Luca Chiapponi

The present article aims to investigate the behaviour of Maxwell–Sutterby fluid past an inclined stretching sheet accompanied with variable thermal conductivity, exponential heat source/sink, magneto-hydrodynamics (MHD), and activation energy. By utilizing the compatible similarity transformations, the nondimensionless PDEs are converted into dimensionless ODEs and further these ODEs are tackled with the help of the bvp4c numerical technique. To check the legitimacy of upcoming results and reliability of the applied bvp4c numerical scheme, a comparison with existing literature and nonlinear shooting method is made. The numerical outcomes delivered here show that the temperature profile escalates due to an augmentation in the heat sink parameter and moreover mass fraction field escalates on account of an improvement in the activation energy parameter.

1. Introduction

The fluids whose viscosity changes due to applied stress are termed as non-Newtonian fluids. Daily life examples of these kind of fluids are ketchup, blood, honey, glue, jellies, etc. Unlike Newtonian fluids, it is complicated to mathematically model the non-Newtonian fluids due to variation in viscosity and elasticity. Many researchers are working to explore the properties like viscosity and elasticity hidden in various non-Newtonian fluids. Prashu and Nandkeolyar [1] utilized finite difference scheme to achieve the numerical solution of three-dimensional Casson fluid under thermal radiation and Hall effect. Saidulu et al. [2] explored the coduct of MHD on radiative tangent hyperbolic nanofluid past an inclined stretchable surface and noticed that the velocity of the fluid diminishes owing to an increment in the magnetic number. Sajid et al. [3] contemplated the impact of heat source/sink and species diffusivity on radiative Reiner–Philippoff fluid past a stretchable surface. Williamson fluid accompanied with MHD, heat source, and nonlinear thermal radiation was deliberated by Parmar [4] who concluded that temperature gradient augments on account of an enhancement in the thermal radiation effect. Wang [5] studied the impact of free convection on vertical stretching surface and noticed that the Nusselt number upsurges because of an augmentation in the Prandtl number. Tlili [6] explored the marvels of MHD, mixed convection, and heat source on Jeffrey fluid flowing across a stretchable surface. They perceived that the temperature field escalates by escalating the magnetic parameter. Khan al. [7] studied the behaviour of non-Newtonian Carreau fluid flow over an inclined surface and found that the fluid velocity diminishes because of an augmentation in the Weissenberg number. Koriko et al. [8] analyzed the conduct of thermal stratification and nonlinear thermal radiation on micropolar fluid moving over a vertical surface. The phenomenon of heat transfer has been investigated by many researchers [9–14].

In recent years, the study of the phenomena like heat generation/absorption and temperature-dependent thermal conductivity has gained interest of the researchers

because of its enormous applications in the field of computer technology and mechanical engineering. The phenomena such as heat source/sink alter the heat distribution which later on make a difference to the particle deposition rate in the system. Heat generation/absorption has immense applications in nuclear reactor engineering, chillers, and heat pumps. The ability of a material to conduct heat is called thermal conductivity. Thermal conductivity's dependence on temperature is termed as variable thermal conductivity. In fluids, thermal conductivity of fluid changes due to intermolecular collision which gives rise to a gradual increase in temperature inside the fluid. Variable thermal conductivity is important in electrolytes which have been important for the preparation of batteries. Various researchers have studied the importance of heat generation/absorption and variable thermal conductivity for the purpose of heat transfer analysis. Patil et al. [15] contemplated the fluid above an exponentially stretching surface along with MHD and nonuniform heat source/sink. They found that temperature profile diminishes by escalating the thermal relaxation effect. Carreau fluid flow under the effect of joule heating and heat source/sink was elucidated by Reddy et al. [16] who determined that an augmentation in the Weissenberg number leads to an enrichment in the temperature distribution. Mahanthesh et al. [17] found the solution of the Casson liquid embedded with exponential temperature-dependent heat source/sink and cross diffusion effects and revealed that an embellishment in the velocity profile occurred by ascending the fluid relaxation effect. Konda et al. [18] studied the Williamson fluid past a vertical sheet with the inclusion of convective heat transfer at the boundary surface along with nonuniform heat source/sink and perceived that the temperature of the fluid abates because of an enrichment in heat sink parameter. Tsai et al. [19] adopted the Chebyshev finite difference scheme to achieve the numerical solution of fluid flowing across a stretchable surface accompanied with nonuniform heat source/sink. Yousif et al. [20] studied radiative Carreau nanofluid flow over an exponentially stretchable embedded with MHD, thermal radiation, and internal heat source/sink and found that the temperature distribution upsurges by mounting the thermal radiation parameter. Kumar and Varma [21] utilized the Runge–Kutta method to achieve the numerical solution of the fluid flow above a porous stretching surface along with suction and internal heat generation/absorption. Abel et al. [22] investigated the viscoelastic fluid flow over a permeable stretching surface together with MHD and heat source/sink. Khan et al. [23] contemplated the impact of heat generation/absorption and MHD on Sisko fluid past a porous stretching sheet. Khan et al. [24] examined the effect of heat source/sink on Maxwell nanofluid flow over a stretchable surface. Irfan et al. [25] scrutinized the behaviour of Maxwell nanofluid influenced by a stretched cylinder embedded with heat source/sink and MHD. Haq et al. [26] scrutinized the impact of heat source/sink and chemical reaction on Cross nanofluid moving over a wedge.

The ability of a material to conduct heat is called thermal conductivity. Thermal conductivity solely depends upon the nature of the material and changes with temperature. Metals have high thermal conductivity in comparison to solids and liquids. In fluids, thermal conductivity depends upon intermolecular collisions of the atoms inside the molecules. As a result of intermolecular collision, the molecules exchange energy with each other and fluid temperature increases which consequently amplifies the thermal conductivity. Thermal conductivity has enormous utilization in the field and technology like electrolytes, steam generators, concrete heating, laminating, catalysis, and molding blow. Gbadeyan et al. [27] analyzed the conduct of variable thermal conductivity and diffusivity on two-dimensional Casson nanofluid past a stretching sheet and found that the temperature field magnifies by amplifying the thermal conductivity parameter. Hamid et al. [28] adopted the Galerkin approach to achieve the numerical solution of nanofluid past a stretchable surface accompanied with variable thermal conductivity. It is noted that the temperature profile escalates as a result of an augmentation in the thermal conductivity parameter. Si et al. [29] contemplated the pseudoplastic fluid moving along a vertical stretching plate embedded with variable thermal conductivity and noted that the mass fraction field augments owing to an embellishment in the power law index. Kumar et al. [30] deliberated the performance hyperbolic tangent fluid with the inclusion of variable thermal conductivity past a sensor stretching surface and found that the velocity field by enhancing the Weissenberg number. Viscous fluid flow between two parallel plates in the presence of variable thermal conductivity, variable viscosity and first order chemical reaction is observed by Umavathi and Shekar [31] and deduced that the temperature profile embellish by embellishing the thermal conductivity variation effect. Salawu and Dada [32] pondered the conduct of inclined magnetic field on incompressible fluid flow over a stretching medium with variable thermal conductivity and found that an escalation in the temperature profile occurred on account of an enrichment in thermal conductivity effect. Lin et al. [33] studied the impact of variable thermal conductivity and thermal radiation on pseudoplastic non-Newtonian nanofluid and found that the temperature distribution increases because of an enlargement in the value of thermal radiation parameter. Aziz et al. [34] scrutinized the conduct of temperature-dependent thermal conductivity and heat generation on inclined radiating plate and observed that the velocity distribution decreases as a result of an improvement in the Prandtl number.

Recently, many researchers studied the influences of electrical conductivity fluid in the presence of magnetic field.

These studies have important applications in generators, pumps, bearings, magneto-hydrodynamic (MHD) generators, etc. One of the basic and important problems in this area is the unsteady magnetic fluid behaviour of boundary layers along fixed or moving stretching surfaces. Khan et al. [35] studied the effect of MHD on Carreau nanofluid moving along a bidirectional stretching surface. They noted that a positive improvement in magnetic parameter increases the temperature field. Sharma and Mishra [36] studied the impact of MHD and internal heat generation/absorption on micropolar fluid moving along a stretchable sheet. Prasad et al. [37] developed a mathematical model of electrical conductivity fluid moving along a slender elastic sheet under the effect of temperature-dependent thermal conductivity, and it is remarkable that a positive amplification in magnetic parameter brings about a decrement in velocity field. Dessie and Kissan [38] investigated heat transfer characteristic of magnetic hydrodynamic fluid past a stretching sheet under the effect of viscous dissipation and heat source/sink utilizing the shooting method. From their numerical study, it is noted that a positive variation in heat sink parameter leads to a reduction in temperature field. Awati [39] scrutinized the behaviour of electrically conducting fluid flow over a stretching sheet accompanied with suction/blowing effects. The effect of variable internal heat generation/absorption and variable thermal conductivity on Carreau fluid moving along a stretchable surface has been debated in detail by Irfan et al. [40]. Mishra et al. [41] analyzed the magneto power law fluid past a porous stretching sheet embedded with nonuniform heat source/sink and found that the velocity of the fluid depreciates owing to an improvement in porosity parameter. Ganga et al. [42] studied the behaviour of MHD on nanofluid past a vertical stretching plate. It is observed that velocity field abates owing to an enhancement in magnetic parameter. Khan et al. [43] contemplated the impact of MHD on Burger's nanofluid past a stretchable surface accompanied with nonlinear thermal radiation and motile gyrotactic microorganisms. Khan et al. [44] studied the impact of MHD and thermal radiation on 3D Sisko fluid moving along a stretchable surface. The impact of MHD on Sisko fluid moving over a stretchable surface embedded with homogenous/heterogenous reaction and thermal radiation has been debated in detail by Khan et al. [45].

The minimum energy provided to the system to start a chemical reaction is called activation energy. Two important energies called kinetic and potential energies are responsible for breaking the bonds during chemical reactions. Sometimes the reaction between molecules are not complete due to the loss of kinetic energy or improper collision. At this stage, minimum amount of energy is needed to start the chemical reaction. Activation energy has distinguished applications in hydrodynamics, geothermal, and oil storage industry. Various researchers studied the marvels of activation energy. Kumar et al. [46] examined the conduct of chemical reaction and activation energy on Carreau fluid and observed that the concentration field increases because of an increment in the activation energy parameter. Gireesha et al. [47] studied the behaviour of activation energy and exponential temperature-dependent heat source on nano-Casson fluid and observed that the concentration distribution depreciates owing to an enhancement in Lewis parameter. Zaib et al. [48] determined the entropy of stagnated nano-Williamson fluid past a moving plate along with activation energy and found that the velocity distribution reduces as a result of an improvement in the Williamson parameter. Alshomrani et al. [49] examined the unsteady Eyring–Powell fluid embedded with MHD and activation energy and observed that the concentration distribution reduces by raising the fitted rate constant parameter. Nanofluid past a stretching sheet along with activation energy and convective boundary conditions was analyzed by Dhlamini et al. [50] who found that the concentration distribution showed a decreasing trend in the case of improvement in the reaction rate constant parameter. Chetteti and Chukka [51] manipulated the consequences of activation energy and convective boundary conditions on nanofluid flow over a cone. They analyzed that the temperature distribution increases by rising the activation energy parameter. Majeed et al. [52] pondered on the impact of activation energy and momentum slip condition on non-Newtonian fluid. They perceived that a positive variation in the Schmidt number abates the fluid concentration. Babu and Sathian [53] treated the water flow through carbon nanotubes along with activation energy. Ahmed and Khan [54] studied the impact of activation energy on Sisko nanofluid moving over a curved surface. The impact of activation energy and binary chemical reaction on 3D Cross nanofluid has been scrutinized in detail by Khan et al. [55]. The impact of activation energy along with nanoparticles on Cross fluid has been discussed by Sultan et al. [56]. Muhammad et al. [57] studied the heat and mass transfer analysis of cross magneto liquid accompanied with thermal conductivity and activation energy. The activation energy was used by many authors to observe its impact on the fluid flow [58–61].

The objective of the present study in the light of above mentioned literature is to explore the importance of various effects on Maxwell–Sutterby fluid flow over an inclined stretching surface. Heat transfer analysis has been carried out in the presence of variable thermal conductivity along with temperature-dependent heat source sink, and both parameters have important applications in energy sector like electrolytes, steam generators, cooling reactors, and nuclear reactors, whereas mass transfer analysis has been debated in the presence of activation energy and variable molecular diffusivity. This paper is important in its sense that no literature has been reported yet to study the mixture of Sutterby and Maxwell fluids past an inclined stretching surface in terms of heat and mass analysis with the aforementioned effects most importantly with variable molecular diffusivity and activation energy.

2. Mathematical Formulation

Two-dimensional incompressible electrically conducting Maxwell–Sutterby fluid flows over a stretching sheet inclined at an angle α under the effect of magnetic field B_0 acting

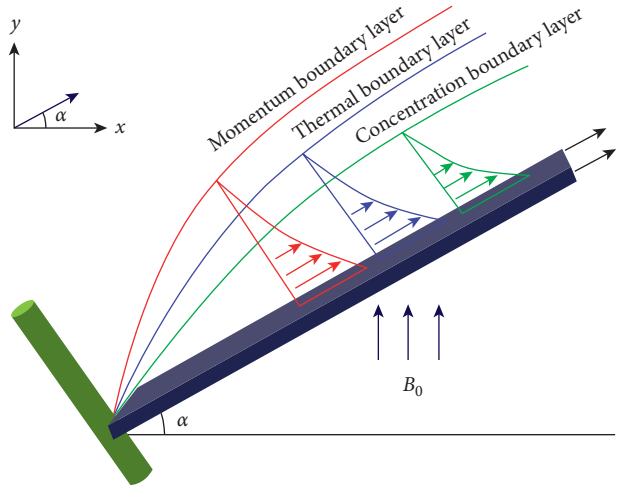

Figure 1: Geometry of the problem.

perpendicular to the sheet as shown in Figure 1. Magnetic field inclination is actually the angle made with the horizontal by the magnetic field lines. Positive values of inclination indicate that the field is pointing downward, into the sheet surface. In this article, the angle of inclination is 45°. It is due to the fact that with an increase in angle of inclination $\alpha = 0°, 45°, 60°, 90°$, the effect of magnetic field on fluid particles increases which enhances the Lorentz force and furthermore depreciates the fluid flow. It is quite notable that maximum resistance is offered for the fluid particles when $\alpha = 90°$. The $x-$ axis is taken along the leading edge of the inclined stretching sheet with stretching velocity $U_w = ax$ and $y-$ axis is normal to the surface. The magnetic Reynolds number is considered very small so that the effect of electric current and induced magnetic field can be neglected as compared to the applied magnetic field. Temperature and concentration at the surface of the sheet are denoted by T_w and C_w, whereas ambient temperature and concentration are indicated by T_∞ and C_∞. The sheet temperature is $T_w > T_\infty$; moreover, fluid concentration is $C_w > C_\infty$. Furthermore, the effects like activation energy, exponential temperature-dependent heat source/sink, and variable thermal and molecular diffusivity are also considered during mathematical formulation of the problem.

Under the aforementioned assumptions and after utilizing the necessary boundary layer approximations the Cartesian form of governing equations regarding continuity, momentum, energy, and concentration are enumerated underneath [10, 13]:

$$\frac{\partial u}{\partial x} + \frac{\partial v}{\partial y} = 0, \tag{1}$$

$$u\frac{\partial u}{\partial x} + v\frac{\partial u}{\partial y} + \lambda_1\left(u^2\frac{\partial^2 u}{\partial x^2} + v^2\frac{\partial^2 u}{\partial y^2} + 2uv\frac{\partial^2 u}{\partial x\,\partial y}\right) = \frac{\nu}{2}\frac{\partial^2 u}{\partial y^2}\left[1 - \frac{Mb^2}{2}\left(\frac{\partial u}{\partial y}\right)^2\right] - \frac{\sigma B_0^2}{\rho}\left(u + \lambda_1 v\frac{\partial u}{\partial y}\right) + \left[g\beta\left(T - T_\infty\right) + g\beta^*\left(C - C_\infty\right)\right]\cos\alpha, \tag{2}$$

$$u\frac{\partial T}{\partial x} + v\frac{\partial T}{\partial y} = \frac{1}{\rho C_p}\frac{\partial}{\partial y}\left(\kappa\frac{\partial T}{\partial y}\right) + \frac{Q_T^*}{\rho C_p}\left(T - T_\infty\right) + \frac{Q_E^*}{\rho C_p}\left(T_w - T_\infty\right)e^{-\sqrt{\left(b/\nu_f\right)}ny}, \tag{3}$$

$$u\frac{\partial C}{\partial x} + v\frac{\partial C}{\partial y} = \frac{\partial}{\partial y}\left(\frac{\partial D_B}{\partial y}\right) - \mathrm{Kr}^2\left(C - C_\infty\right)\left(\frac{T}{T_\infty}\right)^m \exp\left(\frac{-E_a}{\kappa T}\right). \tag{4}$$

The boundary conditions are

$$\left.\begin{aligned} &y = 0: u = u_w(x) = ax,\\ &v = 0,\\ &T = T_w(x),\\ &C = C_w,\\ &y \longrightarrow \infty: u = 0,\\ &T \longrightarrow T_\infty,\\ &C \longrightarrow C_\infty. \end{aligned}\right\} \tag{5}$$

The expression regarding variable thermal conductivity [21] is enumerated below:

$$\kappa = \kappa_\infty(1 + \varepsilon_1\theta), \tag{6}$$

while the variable molecular diffusivity [21] is

$$D_B = D_{B\infty}(1 + \varepsilon_2\phi). \tag{7}$$

By utilizing transformation [9] given below, we convert dimensionless PDEs to nondimensional ODEs.

$$\left.\begin{aligned} u &= axf'(\eta),\\ v &= -\sqrt{a\nu}f(\eta),\\ \eta &= \sqrt{\frac{a}{\nu}}y,\\ \phi(\eta) &= \frac{C - C_\infty}{C_w - C_\infty},\\ \theta(\eta) &= \frac{T - T_\infty}{T_w - T_\infty}. \end{aligned}\right\} \tag{8}$$

After applying similarity transformation, equation (1) satisfies automatically and equations (2)–(4) yield

$$\begin{aligned} &\left[\left(1 - \frac{M}{2}\mathrm{ReDef}''^2\right) - 2\gamma f^2\right]f''' + 4\gamma f f' f'' - 2Hf'\\ &+ 2H\gamma f f'' - 2f'^2 + 2ff'' +\\ &2(\mathrm{Gr}\theta + \mathrm{Br}\phi)\cos\alpha = 0, \end{aligned} \tag{9}$$

$$(1 + \varepsilon_1\theta)\theta'' + \varepsilon_1\theta'^2 + \mathrm{Pr}f\theta' + \mathrm{PrQt}\theta + \mathrm{PrQe}e^{-n\eta} = 0, \tag{10}$$

$$\begin{aligned} &(1 + \varepsilon_2\phi)\phi'' + \varepsilon_2\phi'^2 + \mathrm{Sc}f\phi' - \sigma\mathrm{Sc}(1 + \delta\theta)^m\\ &\cdot \exp\left(\frac{-E}{1 + \delta\theta}\right)\phi = 0. \end{aligned} \tag{11}$$

The boundary conditions are

$$\left.\begin{aligned} &\eta = 0: f(\eta) = 0,\\ &f'(\eta) = 1,\\ &\theta(\eta) = 1,\\ &\phi(\eta) = 1,\\ &\eta \longrightarrow \infty: f'(\eta) \longrightarrow 0,\\ &\theta(\eta) \longrightarrow 0,\\ &\phi(\eta) \longrightarrow 0, \end{aligned}\right\} \tag{12}$$

where

$$\left.\begin{aligned} \gamma &= \lambda_1 a,\\ E &= \left(\frac{E_a}{\kappa T_\infty}\right),\\ \delta &= \frac{T_w - T_\infty}{T_\infty},\\ \mathrm{Re} &= \frac{ax^2}{\nu},\\ \mathrm{De} &= \frac{b^2a^2}{\nu},\\ \mathrm{Sc} &= \frac{\nu}{D_{B_\infty}},\\ H &= \frac{\sigma B_0^2}{\rho a},\\ \mathrm{Qt} &= \frac{Q_T^*}{\rho C_p a},\\ \mathrm{Qe} &= \frac{Q_E^*}{\rho C_p a},\\ \theta_w &= \frac{T_w}{T_\infty},\\ \mathrm{Pr} &= \frac{\nu}{\kappa_\infty},\\ \eta &= \sqrt{\frac{a}{\nu}}y,\\ \mathrm{Gr} &= \frac{g\beta(T_\infty - T_w)}{a^2x},\\ \mathrm{Br} &= \frac{g\beta^*(C_w - C_\infty)}{a^2x},\\ \sigma &= \frac{k_r^2}{a}. \end{aligned}\right\} \tag{13}$$

The skin friction coefficient, rate of heat transfer, and mass transfer on the wall are denoted by

$$Cf_x = \frac{\tau_w}{\rho U_w^2},$$
$$\mathrm{Nu}_x = \frac{xq_w}{k(T_w - T_\infty)}, \tag{14}$$
$$\mathrm{Sh}_x = \frac{xq_m}{D_B(C_w - C_\infty)},$$

whereas the expressions regarding τ_w, q_w, and q_m are given by [13]

$$\left.\begin{aligned} \tau_w &= -\mu\left[(1+\gamma)\frac{\partial u}{\partial y} + \frac{Mb^2}{3}\left(\frac{\partial u}{\partial y}\right)^3\right], \\ q_w &= -\kappa\frac{\partial T}{\partial y}, \\ q_m &= -D_B\left(\frac{\partial C}{\partial y}\right)_{y=0}. \end{aligned}\right\} \tag{15}$$

The dimensionless form of heat transfer and mass transfer is given by

$$\left.\begin{aligned} Cf_x\mathrm{Re}_x^{-1/2} &= -\left[(1+\gamma)f'' + \frac{M}{3}\mathrm{ReDe}f''^3\right], \\ \mathrm{Nu}_x\mathrm{Re}_x^{-1/2} &= -\theta'(0), \\ \mathrm{Sh}_x\mathrm{Re}_x^{-1/2} &= -\phi'(0). \end{aligned}\right\} \tag{16}$$

3. Numerical Scheme

The nonlinear nondimensional transformed problem equations (9)–(11) along with boundary conditions (12) have been solved with the help of the MATLAB built-in function bvp4c [62–64] and nonlinear shooting scheme. In the shooting method, first-order ODEs along with initial conditions are integrated with the utilization of RK4 method and modified missing initial conditions with the utilization of Newton's scheme until solution meets the specified accuracy. The asymptotic convergence is observed to be achieved for $\eta_{\max} = 7$. bvp4c is one of the boundary value problem solvers in MATLAB package. We use MATLAB software where we performed a finite difference method which is a collocation method of order four. All the numerical results achieved in this problem are subjected to an error tolerance 10^{-6}. The system of partial differential equations (PDEs) is converted into first-order ordinary differential equations (ODEs) by utilizing the variables enumerated underneath:

$$\begin{aligned} f &= y_1, \\ f' &= y_2, \\ f'' &= y_3, \\ \theta &= y_4, \\ \theta' &= y_5, \\ \phi &= y_6, \\ \phi' &= y_7. \end{aligned} \tag{17}$$

Thus, equations (9)–(11) become

$$\begin{aligned} y_3' &= \frac{\left[2y_2^2 - 4\gamma y_1 y_2 y_3 + 2H y_2 - 2H\gamma y_1 y_3 - 2y_1 y_3 - 2(\mathrm{Gr}y_4 + \mathrm{Br}y_6)\cos\alpha\right]}{\left[(1 - (M/2)\mathrm{ReDe}y_3^2) - 2\gamma y_1^2\right]}, \\ y_5' &= \frac{-(\mathrm{Pr}y_1 y_5 + \mathrm{PrQt}y_4 + \mathrm{PrQe}e^{-nx} + \varepsilon_1 y_5^2)}{(1 + \varepsilon_1 y_4)}, \\ y_7' &= \left[\frac{\sigma\,\mathrm{Sc}\,(1+\delta y_4)^m \exp(-E/1+\delta y_4)y_6 - \mathrm{Sc}y_1 y_7 - \varepsilon_2 y_5^2]}{(1+\varepsilon_2 y_4),}\right\}, \end{aligned} \tag{18}$$

having boundary conditions enumerated underneath:

$$\left.\begin{aligned} &\eta = 0:\ y_1(0) = 0, \\ &y_2(0) = 1, \\ &y_4(0) = 1, \\ &y_6(0) = 1, \\ &\eta \longrightarrow \infty:\ y_2(\infty) \longrightarrow 0, \\ &y_5(\infty) \longrightarrow 1, \\ &y_7(\infty) \longrightarrow 0. \end{aligned}\right\} \tag{19}$$

To the reader's convenience, a detailed procedure of bvp4c numerical technique is prescribed in Figure 2.

4. Results and Discussion

In this section, the behaviour of various physical parameters emerging during numerical simulation of the problem on the velocity, temperature, and concentration profiles has been debated in the form of graphs, and likewise their impact on skin friction coefficient and heat transfer and mass transfer rate is also discussed in the form of tables. The comparison analysis of numerical results is available in the

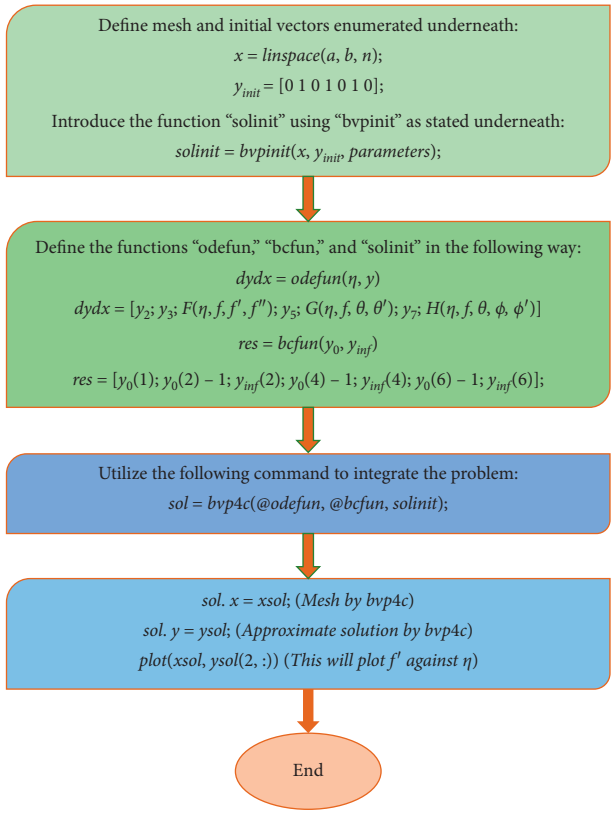

Figure 2: Procedure of numerical scheme bvp4c.

literature. In order to check the authenticity of the numerical scheme and results, a problem can be tackled with nonlinear shooting scheme as well. A comparison analysis of the present scheme with shooting scheme reveals that the computed numerical results are quite reliable and authentic.

Table 1 portrays a comparison analysis of results obtained for $-f''(0)$ with those reported by Ibrahim and Negera [9] by keeping Gr = 0, Br = 0, $\alpha = 0$, $\gamma = -0.14$, $M = 0$, Re = 0, and De = 0.

Table 2 explores the conduct of distinguished parameters on the surface drag coefficient. From the table, it is quite clear that an improvement in parameters such as Maxwell fluid Deborah number γ, magnetic parameter H, Reynolds number Re, Sutterby fluid Deborah number De, angle of inclination α, and power law index M leads to an enhancement in the surface drag coefficient but a variation in the thermal Grashof number Gr and solutal Grashof number Br brings about an abatement in the surface drag coefficient. Table 3 shows the effect of various parameters on the heat transfer and mass transfer rates. From the table, it is observed that an augmentation in the values of Prandtl number Pr, heat source Qt, heat sink Qe, reaction rate constant σ, Schmidt number Sc, exponential index n, temperature difference parameter δ, and thermal conductivity ε_1 produces a decrement in the heat transfer rate, but an improvement in the heat transfer rate is observed on account of an improvement in the fitted rate constant m, activation energy E, and species diffusivity ε_2. The mass transfer rate enlarges because of an augmentation in the values of various

Table 1: Comparison analysis of the obtained results with Ibrahim and Negera [9].

H	Ibrahim and Negera [9]	Present study
0	1.2105	1.1706
0.3	1.3578	1.3393
0.5	1.4478	1.4408
1	1.6504	1.6677

Table 2: Values of the surface drag coefficient $Cf_x\mathrm{Re}_x^{1/2}$ for different parameters.

								$Cf_x\mathrm{Re}_x^{1/2}$	
Gr	Br	α	H	Re	De	γ	M	bvp4c	Shooting
0.2	0.1	0.1	0.1	1	0.1	45°	0.1	1.42862	1.42862
0.3								1.35904	1.35904
0.4								1.29146	1.29146
0.5								1.22556	1.22556
	0.2							1.33346	1.33346
	0.3							1.24192	1.24192
	0.4							1.15328	1.15328
		0.2						1.60140	1.60140
		0.3						1.78077	1.78077
		0.4						1.96660	1.96660
			0.2					1.51040	1.51040
			0.3					1.58891	1.58891
			0.4					1.66451	1.66451
				1.2				1.43062	1.43062
				1.4				1.43262	1.43262
				1.6				1.43462	1.43462
					0.2			1.43865	1.43865
					0.3			1.44879	1.44879
					0.4			1.45907	1.45907
						0°		1.33200	1.33200
						60°		1.49991	1.49991
						90°		1.68932	1.68932
							0.2	1.43865	1.43865
							0.3	1.44879	1.44879
							0.4	1.45907	1.45907

parameters such as Qt, Qe, σ, Sc, n, δ, and ε_1 but mass transfer rate decreases in the case of Pr, m, E, and ε_2.

Figure 3 explores the consequences of solutal Grashof number Br against the velocity profile. Grashof number is actually the ratio of buoyancy forces to the viscous forces. It is quite interesting to note that increasing the value of Br lessens the viscous forces and strengthens the shear forces which eventually improves the velocity field. Figure 4 is sketched to show the impact of Maxwell fluid Deborah number α on the velocity field. The fluids behave like liquids in the case of smaller Deborah number and become more viscous in the case of large values of Deborah number which eventually slows down the fluid velocity and eventually leads to a decrement in the velocity field. Figure 5 is sketched to witness the features of thermal Grashof number Gr on the velocity field. A positive variation in the thermal Grashof number leads to an abatement in the viscous forces which thickens the boundary layer and moreover lessens the velocity profile. The variation of magnetic parameter H on the

Table 3: Values of $\mathrm{Nu}_x\mathrm{Re}_x^{1/2}$ and $\mathrm{Sh}_x\mathrm{Re}_x^{1/2}$ for distinguished parameters.

											$\mathrm{Nu}_x\mathrm{Re}_x^{-1/2}$		$\mathrm{Sh}_x\mathrm{Re}_x^{-1/2}$	
Pr	Qt	Qe	σ	Sc	n	m	δ	E	ε_1	ε_2	bvp4c	Shooting	bvp4c	Shooting
1.7	0.01	0.01	1	0.1	0.1	0.1	0.5	0.5	0.5	0.1	0.5353	0.5353	0.2858	0.2858
1.9											0.5741	0.5741	0.2853	0.2852
2.1											0.6113	0.6113	0.2847	0.2847
2.3											0.6469	0.6469	0.2843	0.2843
	0.03										0.5149	0.5149	0.2860	0.2860
	0.05										0.4937	0.4937	0.2863	0.2863
	0.07										0.4715	0.4715	0.2865	0.2865
		0.03									0.4750	0.4750	0.2873	0.2873
		0.05									0.4158	0.4158	0.2887	0.2887
		0.07									0.3576	0.3576	0.2900	0.2900
			1.1								0.5349	0.5349	0.3054	0.3054
			1.2								0.5340	0.5340	0.3149	0.3149
			1.3								0.5336	0.5336	0.3241	0.3241
				0.2							0.0977	0.0977	0.8197	0.8197
				0.3							0.0973	0.0973	0.8780	0.8780
				0.4							0.0969	0.0969	0.9328	0.9328
					0.2						0.5296	0.5296	0.4015	0.4015
					0.3						0.5256	0.5256	0.4980	0.4980
					0.4						0.5227	0.5227	0.5820	0.5820
						−0.5					0.5356	0.5356	0.2743	0.2743
						0.7					0.5356	0.5356	0.2994	0.2994
						0.9					0.5349	0.5349	0.3044	0.3044
							0.7				0.5352	0.5352	0.2891	0.2891
							1				0.5351	0.5351	0.2934	0.2934
							1.5				0.5350	0.5350	0.2992	0.2992
								0.7			0.5361	0.5361	0.2704	0.2704
								0.9			0.5368	0.5368	0.2567	0.2567
								1.1			0.5374	0.5374	0.2447	0.2447
									0.7		0.4896	0.4896	0.2864	0.2864
									0.9		0.4525	0.4525	0.2868	0.2868
									1.1		0.4217	0.4217	0.2873	0.2873
										0.2	0.5360	0.5360	0.2700	0.2700
										0.3	0.5366	0.5366	0.2564	0.2564
										0.4	0.5372	0.5372	0.2446	0.2446

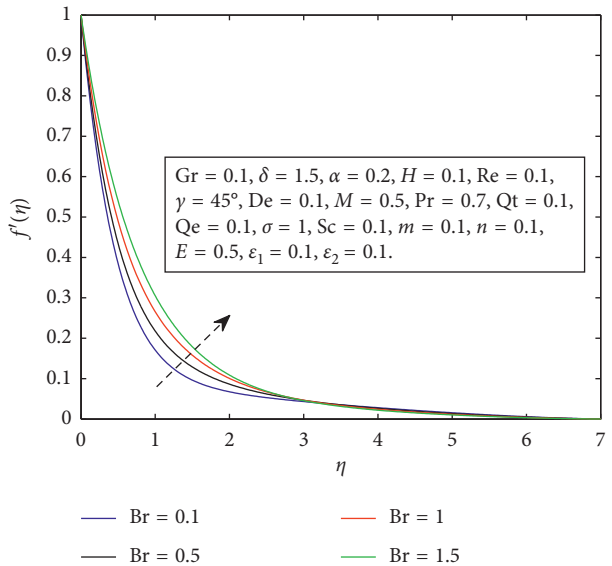

Figure 3: Influence of Br on f'.

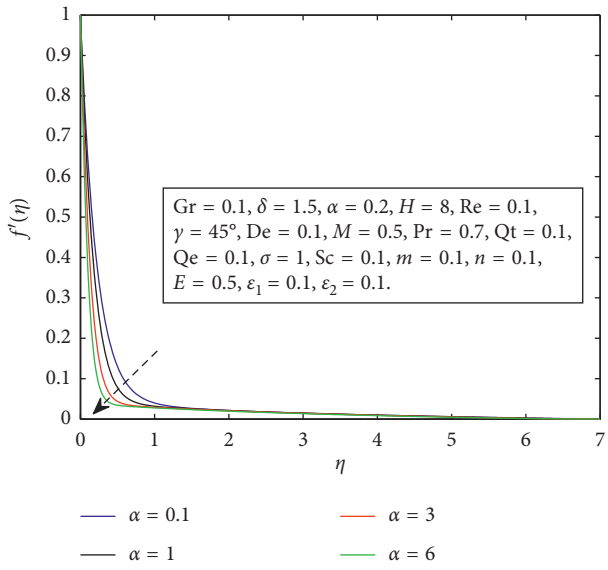

Figure 4: Impact of α on f'.

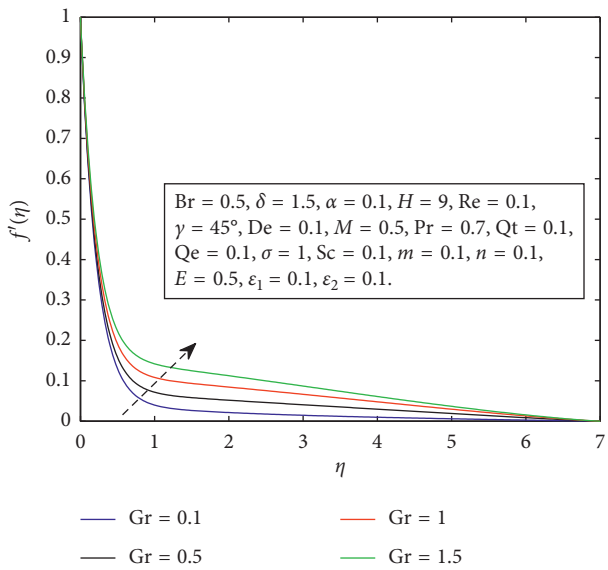

Figure 5: Effect of Gr on f'.

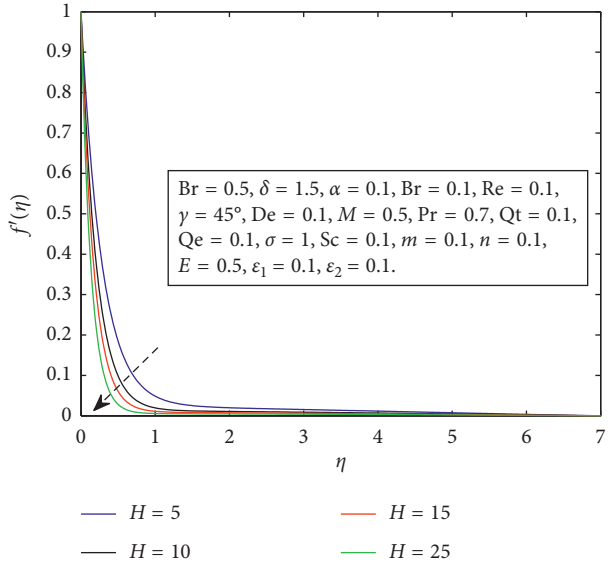

Figure 6: Influence of H on f'.

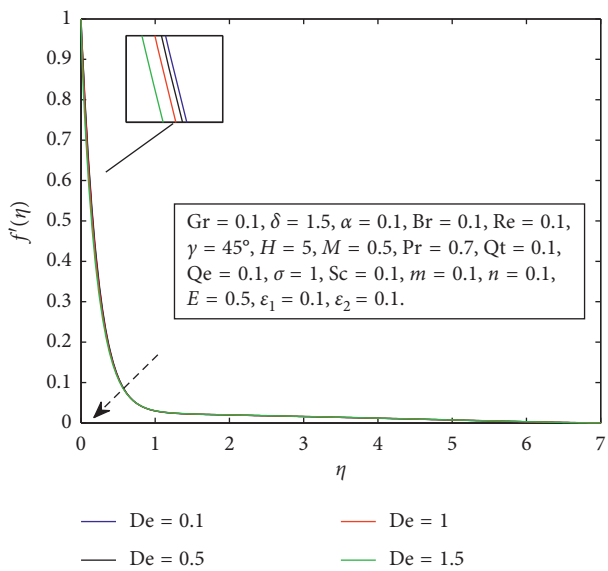

Figure 7: Impact of De on θ.

velocity field is shown in Figure 6. Fluid moving through an electric field in the presence of magnetic field experiences a force called Lorentz force which reduces the movement of the fluid flow. The impact of Sutterby fluid Deborah number De on the velocity profile is shown in Figure 7. Deborah number is defined as the ratio of the characteristic time to the time scale of deformation. The Deborah number is used to represent the viscoelastic nature of the material. It is observed that the greater the Deborah number, the more solid the material; the smaller the Deborah number is, the more fluid it is. From the figure, it is quite clear that an augmentation in the Deborah number brings about an abatement in the fluid movement. As a result, velocity field reduces. Impression of Reynolds number Re on the velocity field is shown in Figure 8. Reynolds number is defined as the ratio of inertial forces to the viscous forces. The fluid becomes more viscous in the case of the higher values of the Reynolds number. The viscous forces dominate the inertial forces which bring about an abatement in the fluid flow. Figure 9 is portrayed to explore the marvels of inclination angle α against the velocity profile. It is revealed that an augmentation in the inclination angle parameter depreciates the buoyancy forces which furthermore reduces the fluid velocity. Figure 10 shows the contribution of power law index m on the velocity field. A shear thinning attitude is observed in liquid in the case of an enhancement in the

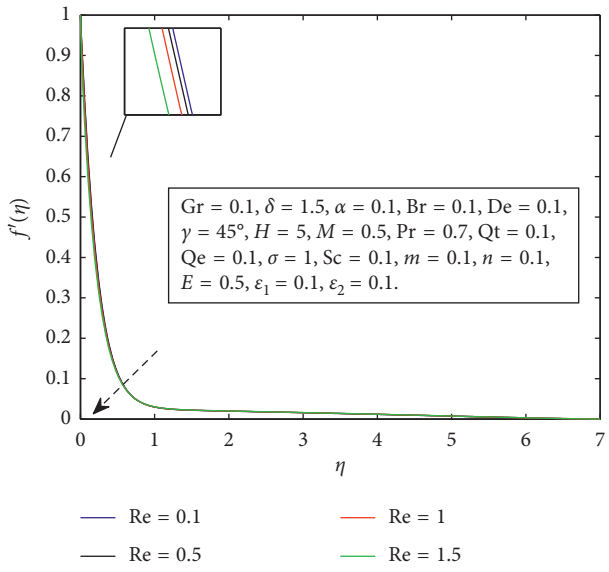

Figure 8: Effect of Re on θ.

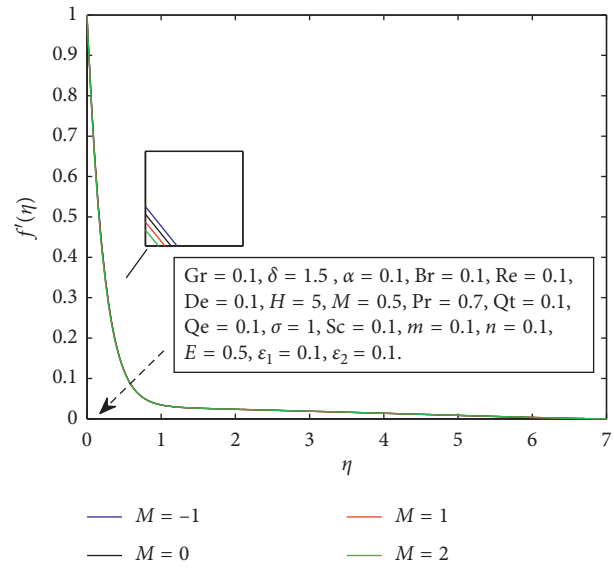

Figure 10: Impact of M on θ.

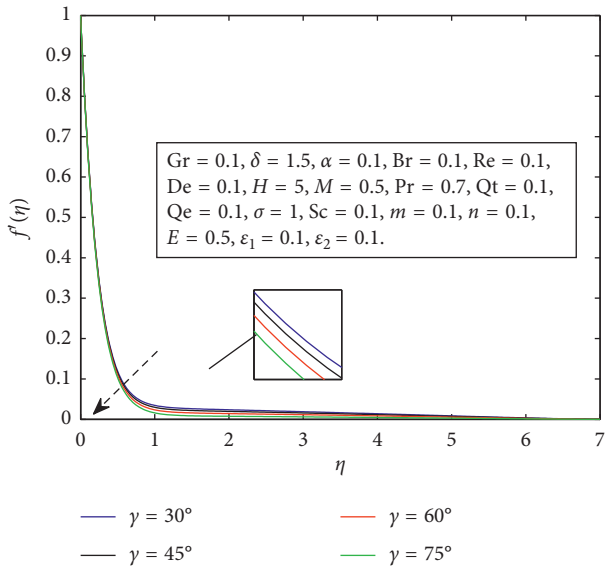

Figure 9: Influence of γ on θ.

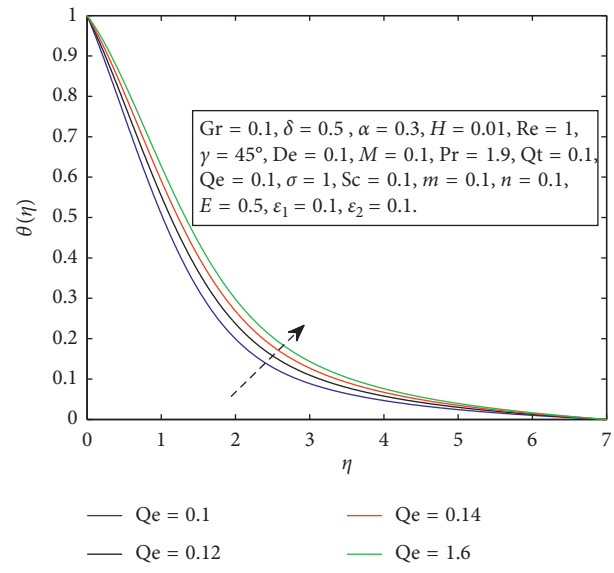

Figure 11: Effect of Qe on θ.

power law index which brings about a reduction in the velocity profile. Figure 11 demonstrates the impact of heat sink parameter Qe on the temperature profile. From the figure, it is quite evident that a positive variation in the heat sink parameter generates more heat into the liquid which leads to an improvement in the thermal boundary layer thickness and temperature profile. Figure 12 is sketched to interpret the features of Pr on the temperature field. Prandtl number is defined as the ratio of momentum diffusivity to the thermal diffusivity. It is quite evident that amplification in thermal diffusivity leads to a reduction in Prandtl number which depreciates the temperature field. Figure 13 demonstrates the conduct of exponential index n on the temperature profile. It is found that a positive variation in n depreciates the heat source/sink term $\mathrm{Qt}\theta + \mathrm{Qe}e^{-n\eta}$ and thermal boundary layer thickness. It is found that a positive variation in the exponential index brings about a decrement in the fluid temperature. Figure 14 shows the influence of thermal conductivity ε_1 on temperature field. It is noteworthy that when the molecules collide with each other, they shift energy which consequently improves the temperature. As a result, an improvement in the thermal conductivity parameter causes amelioration in the fluid temperature and furthermore results in an embellishment in the temperature profile. The impression of reaction rate constant σ on the mass fraction field is shown in Figure 15. It is found that an augmentation in reaction rate constant causes an improvement in the factor $\sigma \mathrm{Sc}(1 + \delta\theta)^m \exp(-E/1 + \delta\theta)$. As a result, destructive chemical reaction occurs and moreover an abatement in the mass fraction field takes place. Figure 16 is

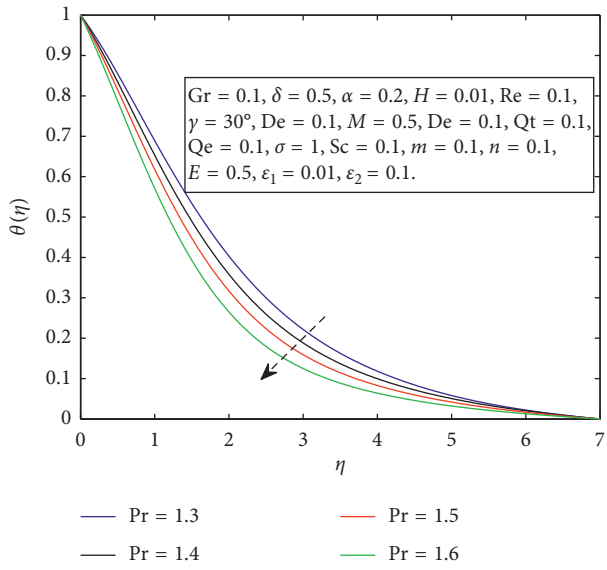

Figure 12: Influence of Pr on θ.

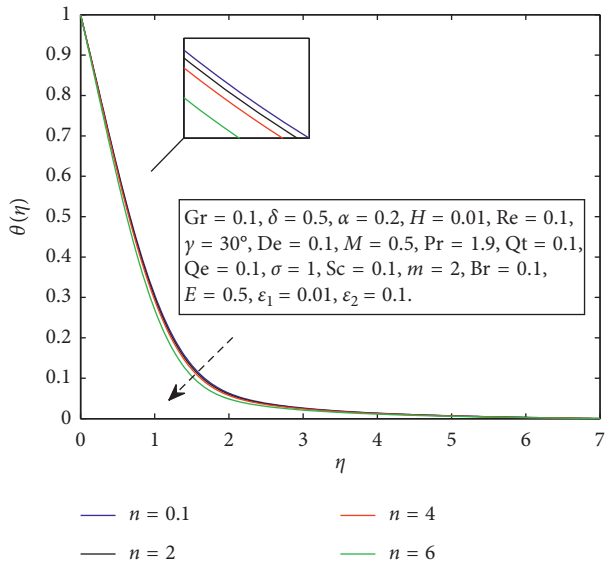

Figure 13: Impact of n on θ.

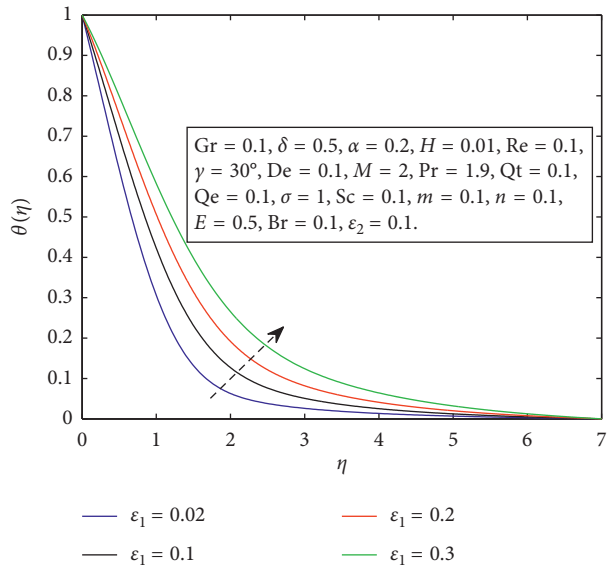

Figure 14: Effect of ε_1 on θ.

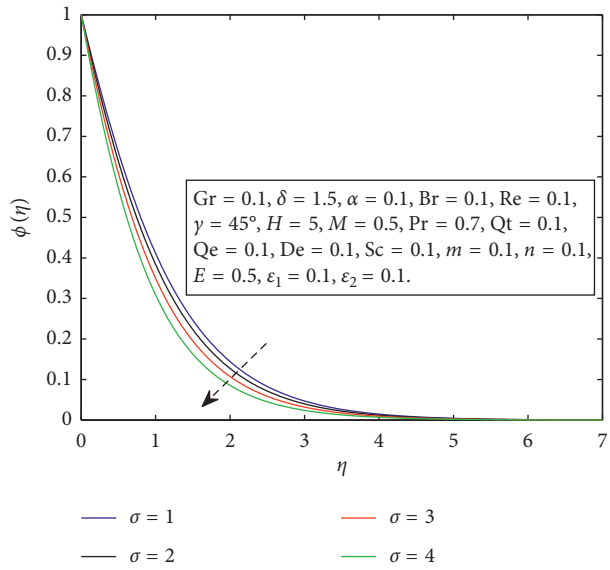

Figure 15: Influence of σ on θ.

designed to depict the effect of Schmidt number Sc on the mass fraction field. Schmidt number is actually the ratio of momentum diffusivity to the Brownian diffusivity. It is observed when molecules collide randomly, the Brownian diffusivity parameter increases which depreciates the Schmidt number. The concentration boundary layer thickness increases due to an improvement in Sc which leads to a reduction in the mass fraction field. Figure 17 explores the conduct of temperature difference parameter δ on the mass fraction field. When the difference between surface temperature and ambient temperature rises, the concentration boundary layer thickness increases which eventually makes a decrement in the mass fraction field. Figure 18 demonstrates the consequences of activation energy E on the mass fraction field. According to the definition, minimum energy required to start a reaction is called activation energy. It is revealed that at lower temperature and high activation energy brings about a decrement in the reaction rate constant which eventually slows down the chemical reaction and furthermore an enhancement in the mass fraction field takes place. Figure 19 shows the behaviour of variable molecular diffusivity ε_2 on the mass fraction field. It is monitored that an augmentation in the species diffusivity ε_2 gives rise to an elevation in the concentration boundary layer thickness. It is also observed that the species diffusivity is directly proportional to the concentration. That is why an embellishment in the mass fraction field takes place as a result of an improvement in species diffusivity parameter. Figure 20 is

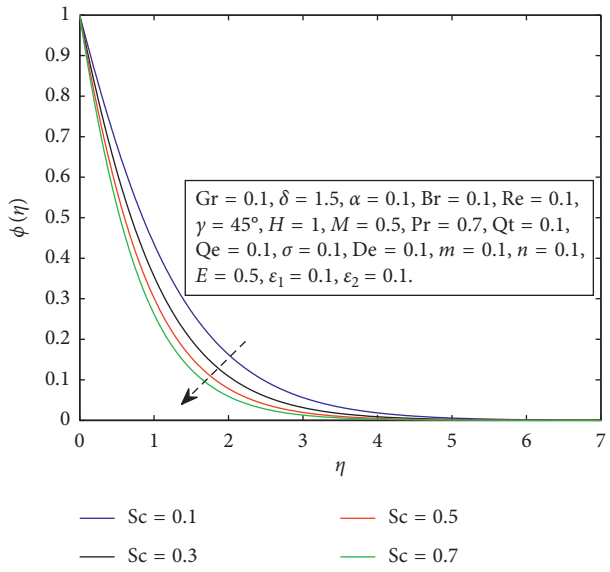

Figure 16: Impact of Sc on θ.

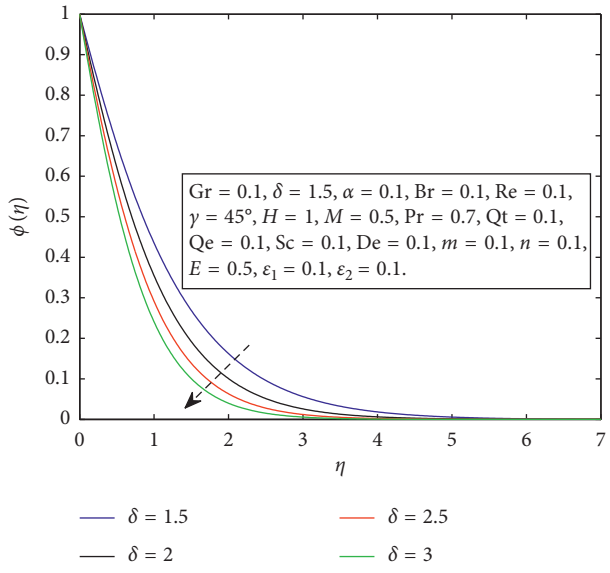

Figure 17: Impact of δ on ϕ.

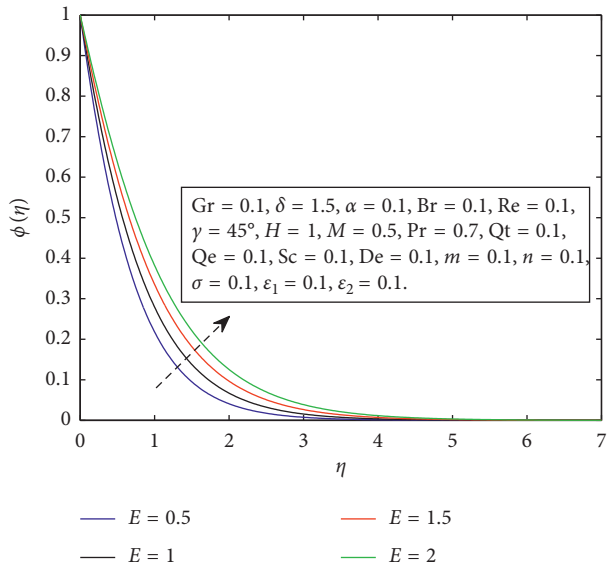

Figure 18: Effect of E on ϕ.

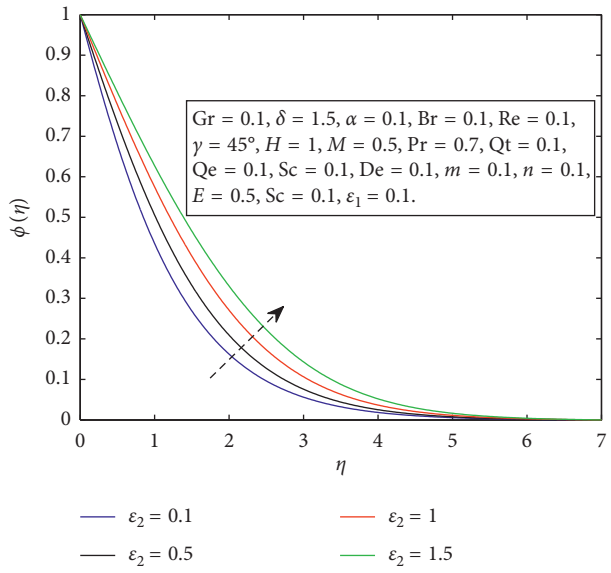

Figure 19: Influence of ε_2 on ϕ.

portrayed to analyze the conduct of fitted rate constant m on the velocity profile. It is found that a boost in m brings about an enhancement in factor $\sigma \mathrm{Sc}(1+\delta\theta)^m \exp(-E/1+\delta\theta)$ which favours the destructive chemical reaction and leads to an increment in the mass fraction field.

5. Final Remarks

The forthright aim of this correspondence is to investigate the influence of exponential temperature dependent-heat source/sink, variable thermal and molecular diffusivity, MHD, and activation energy on Maxwell–Sutterby fluid. The main findings of the present study are enumerated underneath:

(i) The velocity profile $f'(\eta)$ decreases on account of an improvement in magnetic parameter H.

(ii) Shear thickening behaviour is observed on account of an improvement in power law index n.

(iii) The temperature profile $\phi(\eta)$ increases on account of an improvement in the thermal conductivity ε_1, porosity parameter λ, and Deborah number γ.

(iv) Both thermal conductivity parameter ε_1 and the heat sink parameter Qe boost the temperature field.

(v) A positive variation in heat sink Qe depreciates the velocity field.

(vi) An improvement in fitted rate constant m amplifies the concentration field.

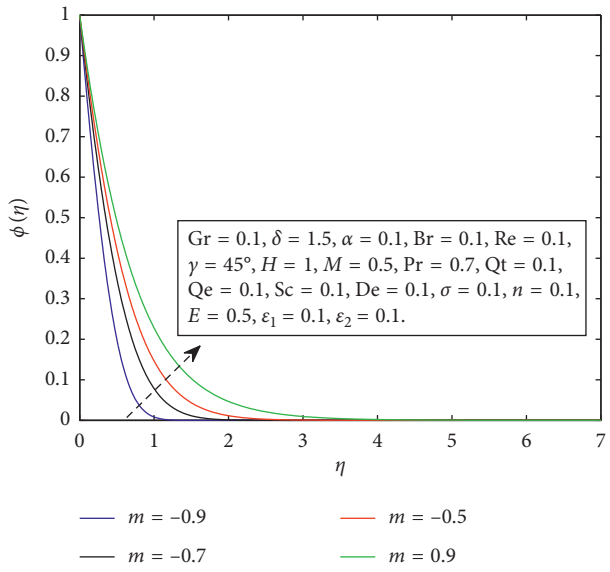

Figure 20: Impact of m on ϕ.

(vii) Mass fraction field $\phi(\eta)$ augments owing to an improvement in E and ε_2.

Nomenclature

Gr: Grashof number
Br: Solutal Grashof number
C: Nanoparticles' concentration
ε_2: Dimensionless thermal conductivity
C_w: Wall concentration
T_∞: Ambient temperature
C_∞: Ambient concentration
u, v: Velocity components
λ_1: Relaxation time
U_w: Stretching velocity
H: Magnetic parameter
De: Deborah number
Re: Reynolds number
ε_2: Species diffusivity
γ: Maxwell fluid Deborah number
α: Inclination angle
j_w: Mass flux
κ: Temperature-dependent thermal conductivity
n: Power law index
q_w: Surface heat flux
Nu_x: Nusselt number
ϕ: Dimensionless concentration
Pr: Prandtl number
Rd: Radiation parameter
E_a: Activation energy
Sc: Schmidt number
σ: Dimensionless reaction rate constant
δ: Temperature difference parameter
m: Fitted rate constant
q_r: Radiative heat flux
B_0: Magnetic field strength
θ_w: Temperature ratio parameter
Kr^2: Reaction rate constant
Q_E^*: Heat sink
Qt: Dimensionless heat source
Qe: Dimensionless heat sink
Q_T^*: Heat source.

Data Availability

No data were used to support this study.

Conflicts of Interest

The authors declare that they have no conflicts of interest.

References

[1] Prashu and R. Nandkeolyar, "A numerical treatment of unsteady three-dimensional hydromagnetic flow of a Casson fluid with Hall and radiation effects," *Results in Physics*, vol. 11, pp. 966–974, 2018.

[2] N. Saidulu, T. Gangaiah, and A. V. Lakshmi, "Radiation effect on MHD flow of a tangent hyperbolic nanofluid over an inclined exponentially stretching sheet," *International Journal of Fluid Mechanics Research*, vol. 46, no. 3, pp. 277–293, 2019.

[3] T. Sajid, M. Sagheer, and S. Hussain, "Impact of temperature-dependent heat source/sink and variable species diffusivity on radiative Reiner–Philippoff fluid," *Mathematical Problems in Engineering*, vol. 202016 pages, 2020.

[4] A. Parmar, "Unsteady convective boundary layer flow for MHD Williamson fluid over an inclined porous stretching sheet with non-linear radiation and heat source," *International Journal of Applied and Computational Mathematics*, vol. 3, no. S1, pp. 859–881, 2017.

[5] C. Y. Wang, "Free convection on a vertical stretching surface," *ZAMM—Journal of Applied Mathematics and Mechanics/ Zeitschrift für Angewandte Mathematik und Mechanik*, vol. 69, no. 11, 1989.

[6] I. Tlili, "Effects of MHD and heat generation on mixed convection flow of Jeffrey fluid in microgravity environment over an inclined stretching sheet," *Symmetry*, vol. 11, no. 3, 2019.

[7] M. Khan, H. Sardar, M. M. Gulzar, and A. S. Alshomrani, "On multiple solutions of non-Newtonian Carreau fluid flow over an inclined shrinking sheet," *Results in Physics*, vol. 8, pp. 926–932, 2018.

[8] O. K. Koriko, I. L. Animasaun, A. J. Omowaye, and T. Oreyeni, "The combined influence of nonlinear thermal radiation and thermal stratification on the dynamics of micropolar fluid along a vertical surface," *Multidiscipline Modeling in Materials and Structures*, vol. 15, no. 1, pp. 133–155, 2018.

[9] W. Ibrahim and M. Negera, "MHD slip flow of upper-convected Maxwell nanofluid over a stretching sheet with chemical reaction," *Journal of the Egyptian Mathematical Society*, vol. 28, no. 7, 2020.

[10] G. K. Ramesh, A. J. Chamkha, and B. J. Gireesha, "MHD mixed convection flow of a viscoelastic fluid over an inclined surface with a non-uniform heat source/sink," *Canadian Journal of Physics*, vol. 93, no. 12, pp. 1138–1143, 2015.

[11] T. Hayat, S. Asad, M. Mustafa, and A. Alsaedi, "Radiation effects on the flow of Powell-Eyring fluid past an unsteady inclined stretching sheet with non-uniform heat source/sink," *PLoS One*, vol. 9, no. 7, Article ID e103214, 2014.

[12] S. S. Ghadikolaei, K. Hosseinzadeh, D. D. Ganji, and B. Jafari, "Nonlinear thermal radiation effect on magneto Casson nanofluid flow with Joule heating effect over an inclined porous stretching sheet," *Case Studies in Thermal Engineering*, vol. 12, pp. 176–187, 2019.

[13] S. Bilal, M. Sohail, R. Naz, M. Y. Malik, and M. Alghamdi, "Upshot of ohmically dissipated Darcy-Forchheimer slip flow of magnetohydrodynamic Sutterby fluid over radiating linearly stretched surface in view of cash and carp method," *Applied Mathematics and Mechanics*, vol. 40, pp. 861–876, 2019.

[14] P. R. Sharma and G. Singh, "Effects of variable thermal conductivity, viscous dissipation on steady MHD natural convection flow of low Prandtl fluid on an inclined porous plate with Ohmic heating," *Meccanica*, vol. 45, no. 2, pp. 237–247, 2010.

[15] P. M. Patil, N. Kumbarwadi, and A. Shashikant, "Effects of MHD mixed convection with non-uniform heat source/sink and crossdiffusion over exponentially stretching sheet," *International Journal of Numerical Methods for Heat and Fluid Flow*, vol. 28, no. 4, 2018.

[16] J. V. R. Reddy, V. Sugunamma, and N. Sandeep, "Simultaneous impacts of Joule heating and variable heat source/sink on MHD 3D flow of Carreau-nanoliquids with temperature dependent viscosity," *Nonlinear Engineering*, vol. 8, no. 1, pp. 356–367, 2018.

[17] B. Mahanthesh, B. J. Gireesha, N. S. Shashikumar, T. Hayat, and A. Alsaedi, "Marangoni convection in Casson liquid flow due to an infinite disk with exponential space dependent heat source and cross-diffusion effects," *Results in Physics*, vol. 9, pp. 78–85, 2018.

[18] J. R. Konda, M. R. Madhusudhana Reddy, R. Konijeti, and A. Dasore, "Effect of non-uniform heat source/sink on MHD boundary layer flow and melting heat transfer of Williamson nanofluid in porous medium," *Multidiscipline Modeling in Materials and Structures*, vol. 15, no. 2, pp. 452–472, 2019.

[19] R. Tsai, K. H. Huang, and J. S. Huang, "Flow and heat transfer over an unsteady stretching surface with non-uniform heat source," *International Communications in Heat and Mass Transfer*, vol. 35, no. 10, pp. 1340–1343, 2008.

[20] M. A. Yousif, H. F. Ismael, T. Abbas, and R. Ellahi, "Numerical study of momentum and heat transfer of MHD Carreau nanofluid over an exponentially stretched plate with internal heat source/sink and radiation," *Heat Transfer Research*, vol. 50, no. 7, pp. 649–658, 2019.

[21] R. V. M. S. S. K. Kumar and S. V. K. Varma, "MHD boundary layer flow of nanofluid through a porous medium over a stretching sheet with variable wall thickness: using Cattaneo–Christov heat flux model," *Journal of Theoretical and Applied Mechanics*, vol. 48, no. 2, pp. 72–92, 2018.

[22] M. S. Abel, M. M. Nandeppanavar, M. B. Malkhed, and M. B. Malkhed, "Hydromagnetic boundary layer flow and heat transfer in viscoelastic fluid over a continuously moving permeable stretching surface with nonuniform heat source/sink embedded in fluid-saturated porous medium," *Chemical Engineering Communications*, vol. 197, no. 5, pp. 633–655, 2010.

[23] M. Khan, L. Ahmad, and M. M. Gulzar, "Unsteady Sisko magneto-nanofluid flow with heat absorption and temperature dependent thermal conductivity: a 3D numerical study," *Results in Physics*, vol. 8, pp. 1092–1103, 2018.

[24] M. Khan, M. Irfan, and W. A. Khan, "Impact of heat source/sink on radiative heat transfer to Maxwell nanofluid subject to revised mass flux condition," *Results in Physics*, vol. 9, pp. 851–857, 2018.

[25] M. Irfan, M. Khan, W. A. Khan, and M. Ayaz, "Modern development on the features of magnetic field and heat sink/source in Maxwell nanofluid subject to convective heat transport," *Physics Letters A*, vol. 382, no. 30, pp. 1992–2002, 2018.

[26] I. Haq, M. Shahzad, W. A. Khan et al., "Characteristics of chemical processes and heat source/sink with wedge geometry," *Case Studies in Thermal Engineering*, vol. 14, Article ID 100432, 2019.

[27] J. A. Gbadeyan, E. O. Titiloye, and A. T. Adeosun, "Effect of variable thermal conductivity and viscosity on (casson) nanofluid flow with convective heating and velocity slip," *Heliyon*, vol. 6, no. 1, Article ID e03076, 2020.

[28] M. Hamid, M. Usman, T. Zubair, R. U. Haq, and W. Wang, "Shape effects of MoS_2 nanoparticles on rotating flow of nanofluid along a stretching surface with variable thermal conductivity: a Galerkin approach," *International Journal of Heat and Mass Transfer*, vol. 124, pp. 706–714, 2018.

[29] X. Si, X. Zhu, L. Zheng, X. Zhang, and P. Lin, "Laminar film condensation of pseudo-plastic non-Newtonian fluid with variable thermal conductivity on an isothermal vertical plate," *International Journal of Heat and Mass Transfer*, vol. 92, pp. 979–986, 2016.

[30] K. G. Kumar, N. G. Rudraswamy, B. J. Gireesha, and S. Manjunatha, "An unsteady squeezed flow of a tangent hyperbolic fluid over a sensor surface in the presence of variable thermal conductivity," *Results in Physics*, vol. 7, pp. 3032–3036, 2017.

[31] J. C. Umavathi and M. Shekar, "Combined effect of variable viscosity and thermal conductivity on free convection flow of a viscous fluid in a vertical channel using DTM," *Meccanica*, vol. 51, no. 1, pp. 71–86, 2016.

[32] S. O. Salawu and M. S. Dada, "Radiative heat transfer of variable viscosity and thermal conductivity effects on inclined magnetic field with dissipation in a non-Darcy medium," *Journal of the Nigerian Mathematical Society*, vol. 35, no. 1, pp. 93–106, 2016.

[33] Y. Lin, L. Zheng, and X. Zhang, "Radiation effects on Marangoni convection flow and heat transfer in pseudo-plastic non-Newtonian nanofluids with variable thermal conductivity," *International Journal of Heat and Mass Transfer*, vol. 77, pp. 708–716, 2014.

[34] A. Aziz, M. Jashim Uddin, M. A. A. Hamad, and A. I. M. Ismail, "MHD flow over an inclined radiating plate with the temperature-dependent thermal conductivity, variable reactive index, and heat generation," *Heat Transfer—Asian Research*, vol. 41, no. 3, pp. 241–259, 2012.

[35] M. Khan, M. Irfan, and W. A. Khan, "Numerical assessment of solar energy aspects on 3D magneto-Carreau nanofluid: a revised proposed relation," *International Journal of Hydrogen Energy*, vol. 42, no. 34, pp. 22054–22065, 2017.

[36] R. P. Sharma and S. R. Mishra, "Effect of higher order chemical reaction on magnetohydrodynamic micropolar fluid flow with internal heat source," *International Journal of Fluid Mechanics Research*, vol. 47, no. 2, pp. 121–134, 2020.

[37] K. V. Prasad, H. Vaidya, and K. Vajravelu, "MHD mixed convection heat transfer over a non-linear slender elastic sheet with variable fluid properties," *Applied Mathematics and Nonlinear Sciences*, vol. 2, no. 2, pp. 351–366, 2017.

[38] H. Dessie and N. Kishan, "MHD effects on heat transfer over stretching sheet embedded in porous medium with variable

viscosity, viscous dissipation and heat source/sink," *Ain Shams Engineering Journal*, vol. 5, no. 3, pp. 967–977, 2014.

[39] V. B. Awati, "Dirichlet series and analytical solutions of MHD viscous flow with suction/blowing," *Applied Mathematics and Nonlinear Sciences*, vol. 2, no. 2, pp. 341–350, 2017.

[40] M. Irfan, M. Khan, and W. A. Khan, "Interaction between chemical species and generalized Fourier's law on 3D flow of Carreau fluid with variable thermal conductivity and heat sink/source: a numerical approach," *Results in Physics*, vol. 10, pp. 107–117, 2018.

[41] S. R. Mishra, S. Baag, G. C. Dash, and M. R. Acharya, "Numerical approach to MHD flow of power-law fluid on a stretching sheet with non-uniform heat source," *Nonlinear Engineering*, vol. 9, no. 1, pp. 81–93, 2019.

[42] B. Ganga, S. M. Y. Ansari, N. Vishnu Ganesh, and A. K. Abdul Hakeem, "MHD flow of Boungiorno model nanofluid over a vertical plate with internal heat generation/absorption," *Propulsion and Power Research*, vol. 5, no. 3, pp. 211–222, 2016.

[43] M. Khan, M. Irfan, and W. A. Khan, "Impact of nonlinear thermal radiation and gyrotactic microorganisms on the magneto-Burgers nanofluid," *International Journal of Mechanical Sciences*, vol. 130, pp. 375–382, 2017.

[44] M. Khan, L. Ahmad, and W. A. Khan, "Numerically framing the impact of radiation on magnetonanoparticles for 3D Sisko fluid flow," *Journal of the Brazilian Society of Mechanical Sciences and Engineering*, vol. 39, no. 11, pp. 4475–4487, 2017.

[45] M. Khan, L. Ahmad, and A. Khan, "Numerical simulation of unsteady 3D magneto-Sisko fluid flow with nonlinear thermal radiation and homogeneous-heterogeneous chemical reactions," *Pramana*, vol. 91, no. 13, 2018.

[46] R. V. M. S. S. K. Kumar, G. V. Kumar, C. S. K. Raju, S. A. Shehzad, and S. V. K. Varma, "Analysis of Arrhenius activation energy in magnetohydrodynamic Carreau fluid flow through improved theory of heat diffusion and binary chemical reaction," *Journal of Physics Communications*, vol. 2, no. 3, Article ID 035004, 2018.

[47] B. J. Gireesha, M. Archana, B. Mahanthesh, and B. C. Prasannakumara, "Exploration of activation energy and binary chemical reaction effects on nano Casson fluid flow with thermal and exponential space-based heat source," *Multidiscipline Modeling in Materials and Structures*, vol. 15, no. 1, pp. 227–245, 2018.

[48] A. Zaib, S. Abelman, A. J. Chamkha, and M. M. Rashidi, "Entropy generation in a Williamson nanofluid near a stagnation point over a moving plate with binary chemical reaction and activation energy," *Heat Transfer Research*, vol. 49, no. 12, pp. 1131–1149, 2018.

[49] A. S. Alshomrani, M. Z. Ullah, S. S. Capizzano, W. A. Khan, and M. Khan, "Interpretation of chemical reactions and activation energy for unsteady 3D flow of eyring-powell magneto-nanofluid," *Arabian Journal for Science and Engineering*, vol. 44, no. 1, pp. 579–589, 2018.

[50] M. Dhlamini, P. K. Kameswaran, P. Sibanda, S. Motsa, and H. Mondal, "Activation energy and binary chemical reaction effects in mixed convective nanofluid flow with convective boundary conditions," *Journal of Computational Design and Engineering*, vol. 6, no. 2, pp. 149–158, 2019.

[51] R. R. Chetteti and V. R. Chukka, "Effects of Arrhenius activation energy and binary chemical reaction on convective flow of a nanoflluid over frustum of a cone with convective boundary condition," *International Journal of Chemical Reactor Engineering*, vol. 16, no. 3, 2017.

[52] A. Majeed, A. Zeeshan, and F. M. Noori, "Numerical study of Darcy-Forchheimer model with activation energy subject to chemically reactive species and momentum slip of order two," *AIP Advances*, vol. 9, no. 4, Article ID 045035, 2019.

[53] J. S. Babu and S. P. Sathian, "The role of activation energy and reduced viscosity on the enhancement of water flow through carbon nanotubes," *The Journal of Chemical Physics*, vol. 134, no. 19, Article ID 194509, 2011.

[54] L. Ahmad and M. Khan, "Importance of activation energy in development of chemical covalent bonding in flow of Sisko magneto-nanofluids over a porous moving curved surface," *International Journal of Hydrogen Energy*, vol. 44, no. 21, pp. 10197–10206, 2019.

[55] W. A. Khan, F. Sultan, M. Ali, M. Shahzad, M. Khan, and M. Irfan, "Consequences of activation energy and binary chemical reaction for 3D flow of cross nanofluid with radiative heat transfer," *Journal of the Brazilian Society of Mechanical Sciences and Engineering*, vol. 41, no. 4, 2019.

[56] F. Sultan, W. A. Khan, M. Ali, M. Shahzad, M. Irfan, and M. Khan, "Theoretical aspects of thermophoresis and Brownian motion for three dimensional flow of the Cross fluid with activation energy," *Pramana*, vol. 92, no. 2, 2019.

[57] S. Muhammad, G. Ali, S. I. A. Shah et al., "Numerical treatment of activation energy for the three dimensional flow of a Cross magnetonanoliquid with variable conductivity," *Pramana Journal of Physics*, vol. 93, no. 40, 2019.

[58] F. G. Awad, S. Motsa, and M. Khumalo, "Heat and mass transfer in unsteady rotating fluid flow with binary chemical reaction and activation energy," *PLoS One*, vol. 9, no. 9, Article ID e107622, 2014.

[59] R. V. M. S. S. K. Kumar, G. V. Kumar, C. S. K. Raju, S. A. Shehzad, and S. V. K. Varma, "Analysis of Arrhenius activation energy in magnetohydrodynamic Carreau fluid flow through improved theory of heat diffusion and binary chemical reaction," *Multidiscipline Modeling in Materials and Structures*, vol. 15, pp. 227–245, 2019.

[60] T. Sajid, M. Sagheer, S. Hussain, and M. Bilal, "Darcy-Forchheimer flow of Maxwell nanofluid flow with nonlinear thermal radiation and activation energy," *AIP Advances*, vol. 8, Article ID 035102, 2018.

[61] D. Lu, M. Ramzan, M. Bilal, J. D. Chung, and U. Farooq, "A numerical investigation of 3D MHD rotating flow with binary chemical reaction, activation energy and non-Fourier heat flux," *Communications in Theoretical Physics*, vol. 70, no. 1, pp. 89–96, 2018.

[62] D. J. Higham and N. J. Higham, *MATLAB Guide*, SIAM, New Delhi, India, 2005.

[63] W. A. Khan and M. Ali, "Recent developments in modeling and simulation of entropy generation for dissipative cross material with quartic autocatalysis," *Applied Physics A*, vol. 125, no. 6, p. 397, 2019.

[64] J. Wang, W. A. Khan, Z. Asghar, M. Waqas, M. Ali, and M. Irfan, "Entropy optimized stretching flow based on non-newtonian radiative nanoliquid under binary chemical reaction," *Computer Methods and Programs in Biomedicine*, vol. 188, Article ID 105274, 2020.